ANALYSIS, DESIGN AND SIMULATION OF PIEZOELECTRIC ACOUSTIC MICROSENSOR

AHMAD KAMAL ARIFFIN MOHD IHSAN[1*], LIM HOCK AUN[2] &
MOHD JAILANI MOHD NOR[3]

Abstract. This paper presents the design analysis, and simulation of piezoelectric acoustic microsensor to imitate outer hair cells (OHCs) inside the human ear. This acoustic microsensor was utilised to develop a new type of microphone. Piezoelectric material PZT 5A was used as the hair cells or beams for the piezoelectric acoustic microsensor. The analysis was conducted using FEMLAB® software to identify the corresponding length to acquire the octave band frequency ranging from 31.5 Hz to 16 kHz. Furthermore, SIMULINK® software was employed to simulate the performance of the acoustic microsensor. The cross section area of the beams was kept at a constant value of 9×9 μm and their length was varied to acquire various resonant frequencies. The suitable lengths, the half power bandwidths and the quality factors of the beams were successfully obtained using FEMLAB®. The simulation procedure was undertaken to obtain sound power level of the beams. The length, half power bandwidth, quality factor and the sound power of the beams are important parameters in designing the acoustic microsensor.

Keywords: Acoustic microsensor, half power bandwidth, octave band frequency, piezoelectric material

Abstrak. Kertas kerja ini membentangkan reka bentuk analisis dan simulasi mikropenderia akustik piezoelektrik untuk meniru tiang-tiang rerambut dalam telinga manusia. Mikropenderia ini dikaji bagi membangunkan mikrofon baru. Bahan piezoelektrik PZT 5A digunakan sebagai tiang-tiang rerambut atau rasuk dalam mikropenderia akustik piezoletrik. Analisis dijalankan menggunakan perisian FEMLAB bagi mengenal pasti panjang rasuk untuk mendapatkan frekuensi jalur oktaf dengan julat 31.5Hz dan 16kHz. Kemudian, perisian SIMULINK pula digunakan bagi menyelaku prestasi mikropenderia akustik. Luas keratan rentas rasuk ditetapkan 9 μm × 9 μm dan panjang pula berubah-ubah bagi mendapatkan pelbagai frekuensi salun. Panjang sesuai lebar jalur kuasa separuh dan faktor kualiti telah berjaya diperolehi menggunakan FEMLAB®. Prosedur penyelakuan telah dijalankan bagi mendapatkan aras kuasa bunyi bagi rasuk. Panjang rasuk, separuh kuasa lebar jalur, faktor kualiti dan kuasa bunyi merupakan parameter penting dalam mereka bentuk mikropenderia akustik.

Kata kunci: Mikropenderia akustik, lebar jalur kuasa separuh, frekuensi jalur oktaf, bahan piezoletrik

[1,2&3] Computational Mechanics Research Group, Department of Mechanical and Materials Engineering, Universiti Kebangsaan Malaysia, 43600 Bangi, Selangor, Malaysia

* Corresponding author: Email: kamal@eng.ukm.my

1.0   INTRODUCTION

The development of piezoelectric materials has constituted a revolution in sensing and actuation applications in recent years [1]. Piezoelectric materials have the advantages that they can be used for both sensing and actuation [2]. The rapidly responding ability, broad frequency band, little power consumption, high sensitivity and stability properties make piezoelectric materials increasingly popular [3]. The piezoelectric materials, especially lead zirconate titanate (PZT) ceramics, have been used in numerous applications such as sensors, actuators and micro-electro-mechanical system (MEMS) [4-12]. The most important property of piezoelectric materials is their strong coupling between electric and mechanical constitutive behavior [13]. When mechanical pressure is applied to the piezoelectric materials, the piezoelectric materials will produce voltage as a function of the applied pressure. Conversely, when an electric field is applied, the structure changes shape producing dimensional changes in the material [14,15].

    This paper focuses on the analysis, design and simulation of piezoelectric acoustic microsensor to imitate outer hair cells (OHCs) inside the human ear. Piezoelectric material PZT 5A was used as the beams for this new type of microphone. FEMLAB$^{®}$ software was used for analysis and SIMULINK$^{®}$ software was employed to simulate the performance of the acoustic microsensor. The suitable lengths, the half power bandwidths and the quality factors of the beams are obtained using FEMLAB$^{®}$ and the simulation procedure was undertaken to obtain sound power level of the beams.

2.0   THEORETICAL ASPECTS

2.1   Piezo-electrostatic Constitutive Relationship

Electrostatic computation is coupled to a structural mechanical computation via a piezo-electrical constitutive relationship. The constitutive equations for structural mechanics and electrostatic are as follows [16-27]:

$$\boldsymbol{\sigma} = \mathbf{C}\boldsymbol{\epsilon} - \mathbf{e}\mathbf{E} \tag{1}$$

$$\mathbf{D} = \mathbf{e}^{\mathbf{T}}\boldsymbol{\epsilon} + k\mathbf{E} \tag{2}$$

where $\boldsymbol{\sigma}$, $\boldsymbol{\epsilon}$, $\mathbf{E}$ and $\mathbf{D}$ denote the vectors of stress, strain, electric field and electric displacement, respectively while $\mathbf{C}$, $\mathbf{e}$ and k denote the matrices of elastic stiffness, piezoelectric coupling and dielectric permittivity, respectively.

    The number of independent coefficients in Equations (1) and (2) depends on the material symmetry. The constitutive equations for plane stress case of a piezoelectric ceramic with the axis of polarization collinear with the vertical axis (y-axis) can be expressed as [2]:

$$
\begin{pmatrix} \sigma_x \\ \sigma_y \\ \tau_{xy} \end{pmatrix} = \begin{pmatrix} \left(c_{11}-\dfrac{c_{12}^{2}}{c_{11}}\right) & \left(c_{13}-\dfrac{c_{13}c_{12}}{c_{11}}\right) & 0 \\ \left(c_{13}-\dfrac{c_{13}c_{12}}{c_{11}}\right) & \left(c_{33}-\dfrac{c_{13}^{2}}{c_{11}}\right) & 0 \\ 0 & 0 & c_{44} \end{pmatrix} \begin{pmatrix} \varepsilon_x \\ \varepsilon_y \\ \gamma_{xy} \end{pmatrix} - \begin{pmatrix} 0 & \left(e_{31}-\dfrac{c_{12}e_{31}}{c_{11}}\right) \\ 0 & \left(e_{33}-\dfrac{c_{13}e_{31}}{c_{11}}\right) \\ e_{15} & 0 \end{pmatrix} \begin{pmatrix} E_x \\ E_y \end{pmatrix} \quad (3)
$$

$$
\begin{pmatrix} D_x \\ D_y \end{pmatrix} = \begin{pmatrix} 0 & 0 & e_{15} \\ \left(e_{31}-\dfrac{c_{12}e_{31}}{c_{11}}\right) & \left(e_{33}-\dfrac{c_{13}e_{31}}{c_{11}}\right) & 0 \end{pmatrix} \begin{pmatrix} \varepsilon_x \\ \varepsilon_y \\ \gamma_{xy} \end{pmatrix} + \begin{pmatrix} \varepsilon_{11} & 0 \\ 0 & \left(\varepsilon_{33}+\dfrac{e_{31}^{2}}{c_{11}}\right) \end{pmatrix} \begin{pmatrix} E_x \\ E_y \end{pmatrix} \quad (4)
$$

where σ_x and σ_y denote the stress components, τ_{xy} denotes the shear stress component, ε_x and ε_y denote the strain components, γ_{xy} denotes the shear strain component, E_x and E_y denote the electric field components, D_x and D_y denote the electric displacement components, c_{11}, c_{13}, c_{33} and c_{44} denote the elastic stiffness coefficients, e_{15}, e_{31} and e_{33} denote the piezoelectric coupling coefficients for stress-charge form, while ε_{11} and ε_{33} denote the dielectric permittivity coefficients.

Equations (3) and (4) are substituted into the electrostatic equation and the two equibrilium equations for structural mechanics [2, 28]:

$$
-\frac{\partial}{\partial x}(D_x) - \frac{\partial}{\partial y}(D_y) = 0 \quad (5)
$$

$$
\rho\left(\frac{\partial^2 u}{\partial t^2}\right) - \frac{\partial \sigma_x}{\partial x} - \frac{\partial \tau_{xy}}{\partial y} = 0 \quad (6)
$$

$$
\rho\left(\frac{\partial^2 v}{\partial t^2}\right) - \frac{\partial \tau_{xy}}{\partial x} - \frac{\partial \sigma_y}{\partial y} = 0 \quad (7)
$$

where ρ is the density of piezoelectric ceramic material.

The unknown to be solved for are the two displacements u and v together with the potential V. The further relationships required are the strain-displacement relations and the electrostatic field as a function of the potential [2, 28-30]:

$$
\varepsilon_x = \frac{\partial u}{\partial x} \quad (8)
$$

$$
\varepsilon_y = \frac{\partial v}{\partial y} \quad (9)
$$

$$
\gamma_{xy} = 2\varepsilon_{xy} = \frac{\partial u}{\partial y} + \frac{\partial v}{\partial x} \quad (10)
$$

$$E_x = -\frac{\partial V}{\partial x} \tag{11}$$

$$E_y = -\frac{\partial V}{\partial y} \tag{12}$$

For plane stress case of a piezoelectric ceramic, without losing generality, the axis of polarization is assumed collinear with the horizontal axis (x-axis), the constitutive equations analogous to Equations (3) and (4) become [24]:

$$
\begin{pmatrix} \sigma_y \\ \sigma_x \\ \tau_{xy} \end{pmatrix} =
\begin{pmatrix}
\left(c_{11} - \frac{c_{12}{}^2}{c_{11}}\right) & \left(c_{13} - \frac{c_{13}c_{12}}{c_{11}}\right) & 0 \\
\left(c_{13} - \frac{c_{13}c_{12}}{c_{11}}\right) & \left(c_{33} - \frac{c_{13}{}^2}{c_{11}}\right) & 0 \\
0 & 0 & c_{44}
\end{pmatrix}
\begin{pmatrix} \varepsilon_y \\ \varepsilon_x \\ \gamma_{xy} \end{pmatrix} -
\begin{pmatrix}
0 & \left(e_{31} - \frac{c_{12}e_{31}}{c_{11}}\right) \\
0 & \left(e_{33} - \frac{c_{13}e_{31}}{c_{11}}\right) \\
e_{15} & 0
\end{pmatrix}
\begin{pmatrix} E_y \\ E_x \end{pmatrix} \tag{13}
$$

$$
\begin{pmatrix} D_y \\ D_x \end{pmatrix} =
\begin{pmatrix}
0 & 0 & e_{15} \\
\left(e_{31} - \frac{c_{12}e_{31}}{c_{11}}\right) & \left(e_{33} - \frac{c_{13}e_{31}}{c_{11}}\right) & 0
\end{pmatrix}
\begin{pmatrix} \varepsilon_y \\ \varepsilon_x \\ \gamma_{xy} \end{pmatrix} +
\begin{pmatrix}
\varepsilon_{11} & 0 \\
0 & \left(\varepsilon_{33} + \frac{e_{31}{}^2}{c_{11}}\right)
\end{pmatrix}
\begin{pmatrix} E_y \\ E_x \end{pmatrix} \tag{14}
$$

2.2 Rayleigh Damping

Damping is modeled using Raleigh damping parameters with damping coefficients proportional to the mass and stiffness in the following way [31]:

$$C = \alpha_{dm}M + \beta_{dK}K \tag{15}$$

where C denotes the Rayleigh damping, M donotes the mass, K denotes the stiffness, while α_{dM} and β_{dK} denote Rayleigh damping parameters.

In order to specify values for the damping, the relations between critical damping ratio and damping parameters can be used. The critical damping ratios are more defined and given by [31]:

$$\xi_i = \frac{\dfrac{\alpha_{dM}}{\omega_i} + \beta_{dK}.\omega_i}{2} \tag{16}$$

where ξ_i is the critical damping ratio at a specific angular frequency ω_i.

$$\text{If } i = 1, \xi_1 = \frac{\dfrac{\alpha_{dM}}{\omega_1} + \beta_{dK}.\omega_1}{2} = \frac{1}{(2.\omega_1)}\alpha_{dM} + \frac{\omega_1}{2}\beta_{dK} \tag{16a}$$

$$\text{If } i = 2, \xi_2 = \frac{\dfrac{\alpha_{dM}}{\omega_2} + \beta_{dK}.\omega_2}{2} = \frac{1}{(2.\omega_2)}\alpha_{dM} + \frac{\omega_2}{2}\beta_{dK} \tag{16b}$$

Knowing two pairs of corresponding ξ_i and ω_i results in a system of equations:

$$\begin{Bmatrix} \xi_1 \\ \xi_2 \end{Bmatrix} = \begin{bmatrix} \dfrac{1}{2\omega_1} & \dfrac{\omega_1}{2} \\ \dfrac{1}{2\omega_2} & \dfrac{\omega_2}{2} \end{bmatrix} \begin{Bmatrix} \alpha_{dM} \\ \beta_{dK} \end{Bmatrix} \tag{17}$$

2.3 Sound Power Level

The sound power level (PWL) for the piezoelectric acoustic microsensor can be expressed as [32]:

$$\text{PWL (dB)} = 10 \log_{10} \frac{V^2}{V_r^2} \tag{18}$$

where V is the maximum electric potential produced by the beam and V_r is the maximum electric potential produced by the beam at its resonance frequency.

2.4 Half Power Bandwidth and Quality Factor

The half power bandwidth refers to the beam's useful range of operating frequencies. In practice, this half power bandwidth is found by measuring the amplitude at the center frequency and then finding the width at an amplitude that is 3 decibels below the amplitude at the center frequency [33], which is illustrated in Figure 1.

The quality factor, Q, describes the sharpness of the beam's response. The quality factor is equal to the ratio of the center frequency to the bandwidth [34]:

$$Q = \frac{F0}{F2 - F1} \tag{19}$$

where $F0$ denotes the center frequency of the beam and $(F2 - F1)$ denotes the half power bandwidth of the beam. The larger the value of Q, the less dissipative effect and the greater the number of cycles of free oscillation for a given decrease of amplitude [34].
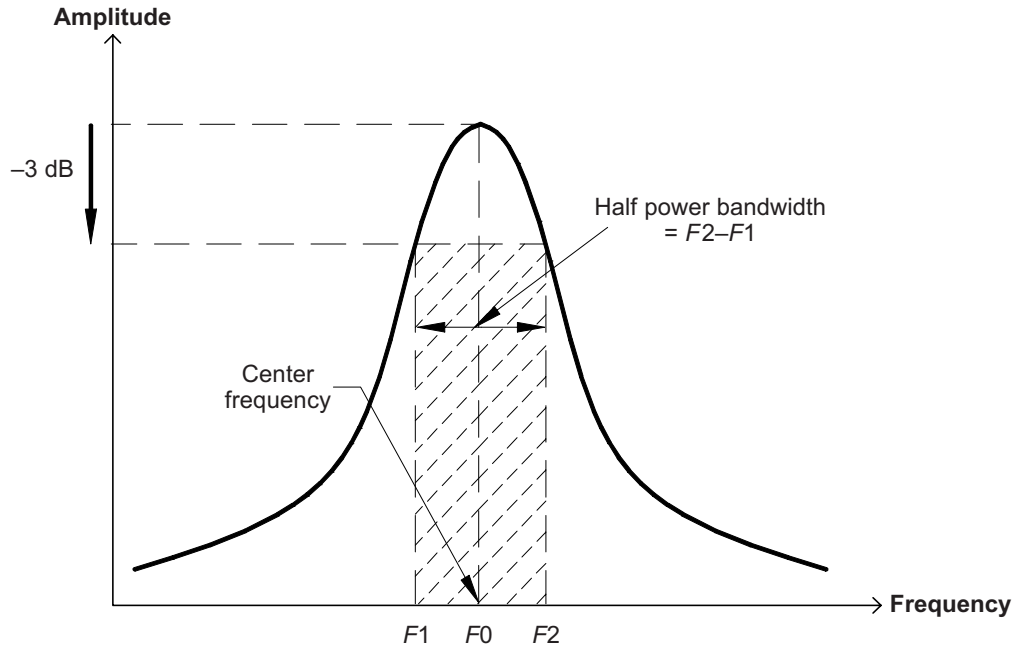
Figure 1   Center frequency and half power bandwidth

3.0   PIEZOELECTRIC BEAM MODEL

Piezoelectric material PZT 5A was selected to produce the beams for the piezoelectric acoustic microsensor. The material properties for PZT 5A is given in Table 1. The cross section area of the beams was kept at a constant value of 9×9 µm but their lengths were varied according to resonant frequencies. This is similar to the outer

Table 1   PZT 5A properties [42-45]

Elastic Stiffness Coefficients (GPa)	
c_{11}	121.00
c_{12}	75.40
c_{13}	75.20
c_{33}	111.00
c_{44}	21.10
Piezoelectric Coefficients (C/m^2)	
e_{31}	–5.40
e_{33}	15.80
e_{15}	12.30
Dielectric Constants (10^{-9} F/m)	
ε_{11}	8.107
ε_{33}	7.346

hair cells (OHCs) inside the human ear [15] which the diameter of OHCs is 9 μm [35-40]. The beams with different resonant frequencies were used to identify sound signals at the octave band frequency ranging from 31.5 Hz to 16 kHz [41].

FEMLAB® software was used for the eigen frequency and frequency response analysis to calculate the lengths, half power bandwidths and quality factors of the beams. Whereas SIMULINK® software was employed to simulate the performance of the acoustic microsensor. The beams were modeled in plane stress using FEMLAB® software and the piezoelectric medium was assumed to be hexagonally symmetric or polarized along the horizontal axis (*x*-axis) (Figure 2). In the frequency response analysis, all the beams were applied the same pressure of 0.02 Pa on the left along the beam in different range of frequencies.
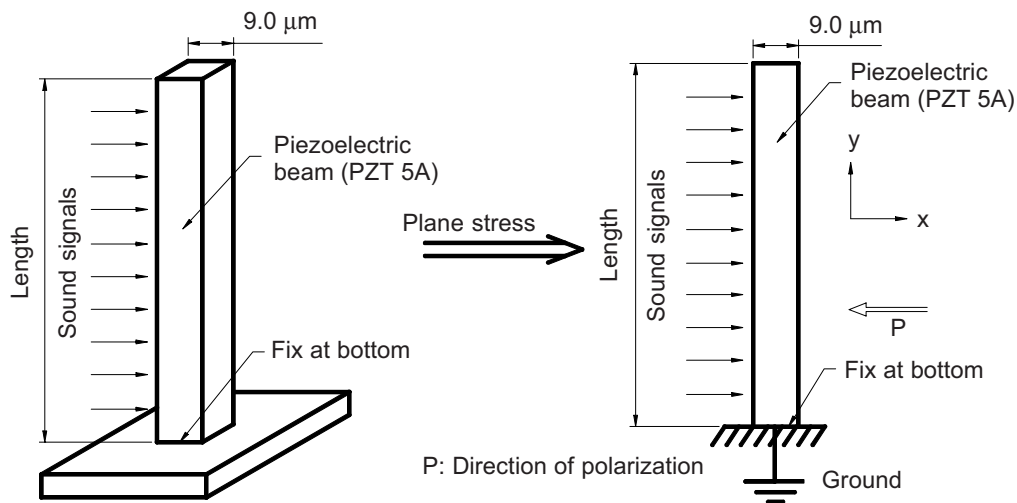
Figure 2   Piezoelectric beam

4.0   NUMERICAL RESULTS AND DISSCUSSION

4.1   Resonant Frequency Analysis

Resonant frequency is a natural frequency of vibration determined by the physical parameters of the vibrating object. The beams were vibrated most efficiently at their resonant frequency and produce the highest electrical potential. While the cross section area of the beams was kept at a constant value of 9×9 μm, their length was varied according to resonant frequencies (Figure 3). The decreasing of the beam's length caused the resonant frequency of the beam to increase. The longest beam (Beam 1) has the resonant frequency at 31.5 Hz and the shortest beam (Beam 10) has the resonant frequency at 16 kHz.
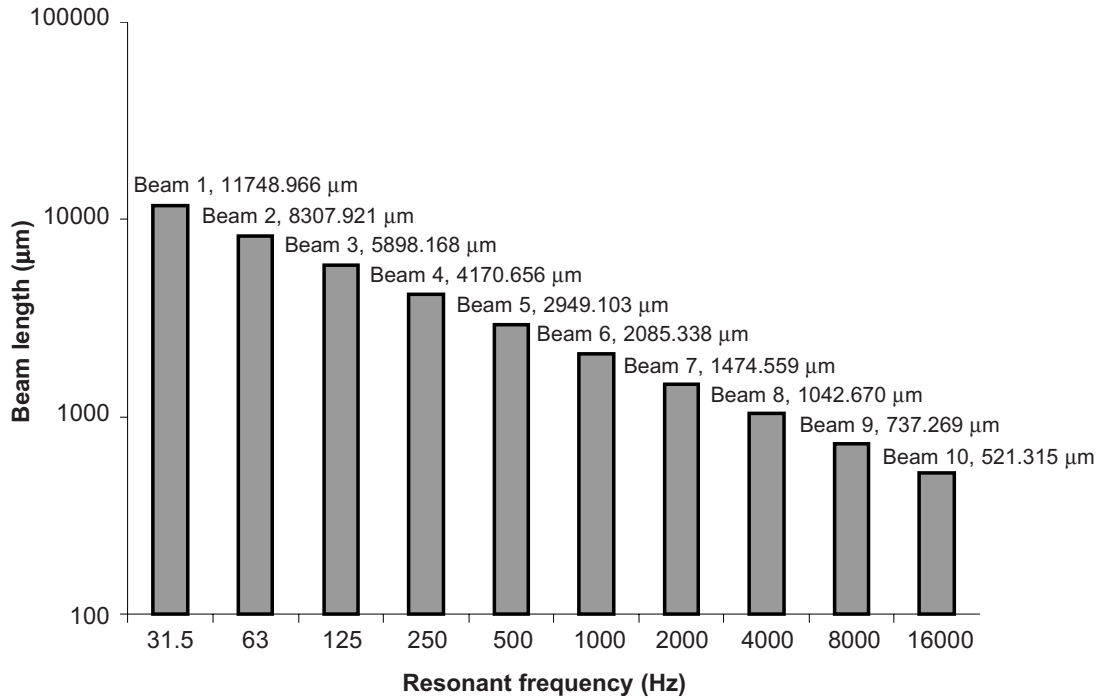
Figure 3   Beam length according to resonant frequency

4.2 **Frequency Response Analysis**

Damping was modeled using Rayleigh damping and the critical damping was assumed as 1%. The range of applied frequencies and the values of α_{dM} and β_{dK} for different beams are shown in Table 2. Figure 4 shows the maximum electric potential produced by Beam 10 at its resonant frequency of 513 μV. The maximum electric potential produced by Beam 10 at the range of its applied frequencies is shown in Figure 5.

Table 2   Range of applied frequencies and values of α_{dm} and β_{dk} for different beams

	Range of applied frequencies (Hz)	α_{dm}	β_{dk}
Beam 1	26.5 – 36.5	1.9293	5.05E-05
Beam 2	58 – 68	3.9335	2.53E-05
Beam 3	115 –135	7.8037	1.27E-05
Beam 4	225 – 275	15.5509	6.37E-06
Beam 5	450 – 550	31.1018	3.18E-06
Beam 6	900 – 1100	62.2035	1.59E-06
Beam 7	1750 – 2250	123.7002	7.96E-07
Beam 8	3500 – 4500	247.4004	3.98E-07
Beam 9	7000 – 9000	494.8008	1.99E-07
Beam 10	14000 – 18000	938.2890	1.06E-07
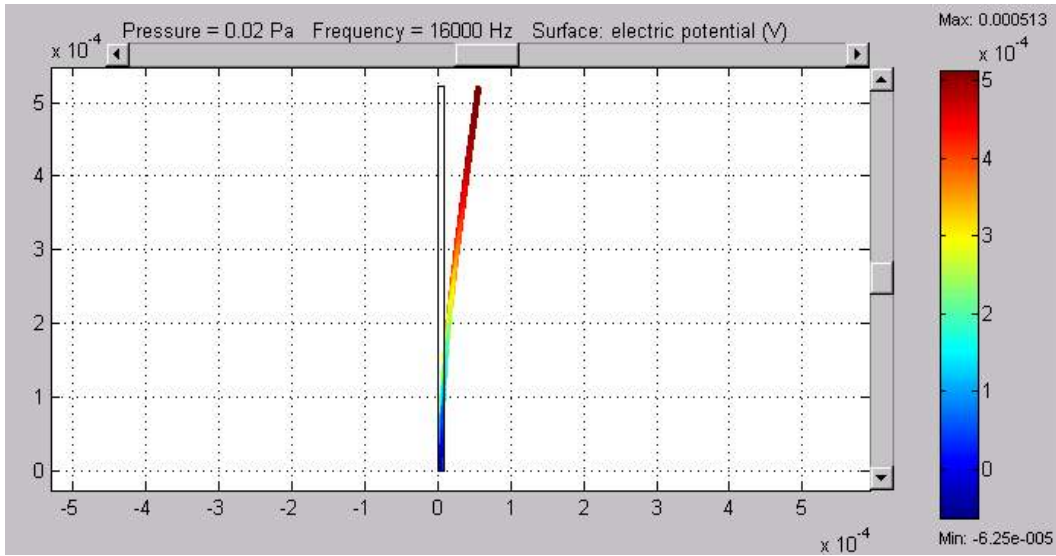
Figure 4   Electric potential produced by Beam 10 at 16 kHz
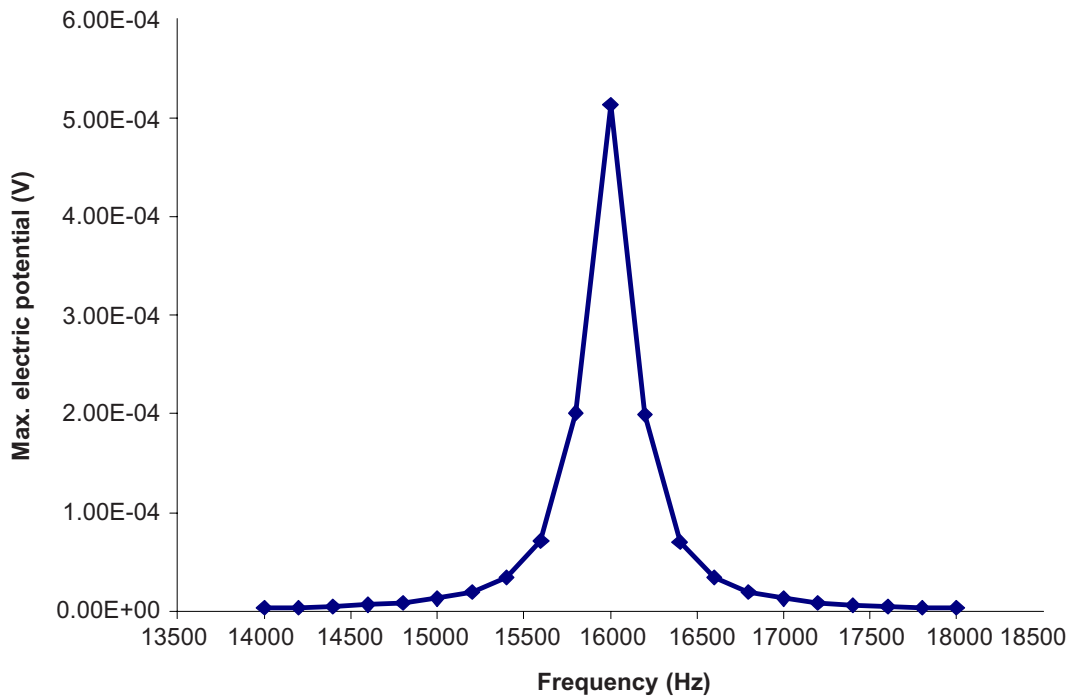
Figure 5   Maximum electric potential produced by Beam 10 at the range of its applied frequencies

AHMAD KAMAL ARIFFIN, LIM HOCK AUN & MOHD JAILANI
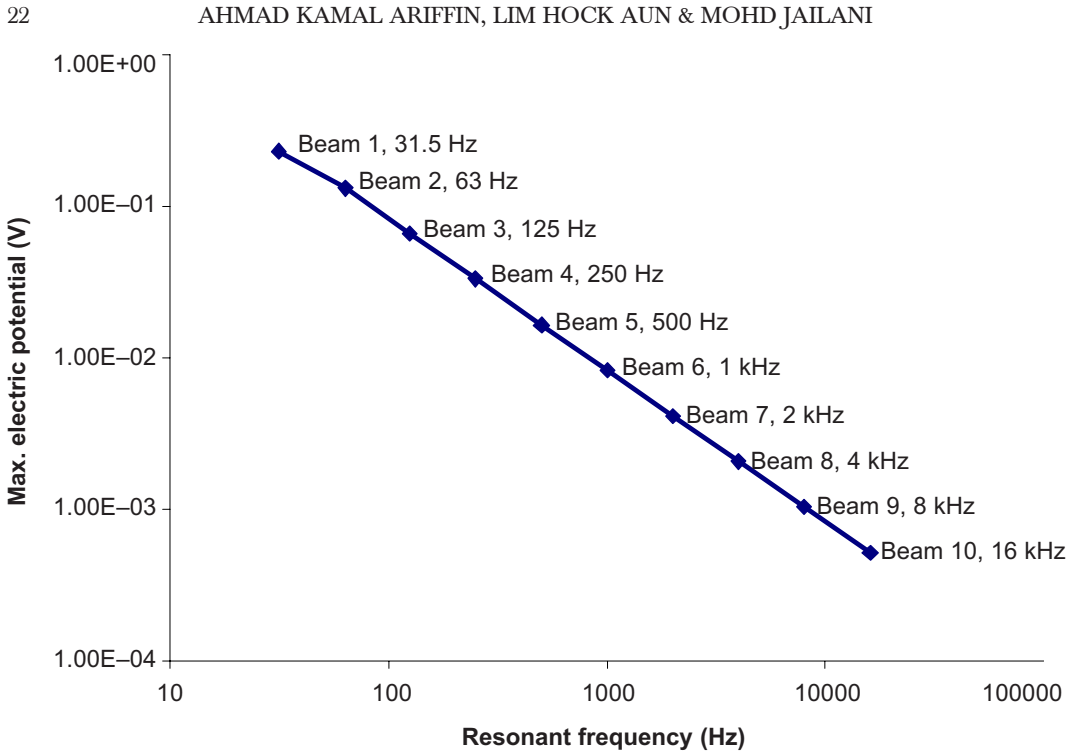
Figure 6   Maximum electric potential produced by different beams at its resonant frequency

The maximum electric potential produced by long beam at its resonant frequency is higher than the short beam (Figure 6).

The electric potential was converted to sound power level using Equation (18). Figure 7 shows the sound power level for Beam 10 at the range of its applied frequencies. The half power bandwidth and quality factor for Beam 10 could be

Table 3   Half power bandwidth and quality factor for different beams

	Half power bandwidth (Hz)	Quality factor, Q
Beam 1	0.40	78.75
Beam 2	0.77	81.82
Beam 3	1.50	83.33
Beam 4	3.00	83.33
Beam 5	6.00	83.33
Beam 6	12.50	80.00
Beam 7	25.00	80.00
Beam 8	50.00	80.00
Beam 9	100.00	80.00
Beam 10	200.00	80.00
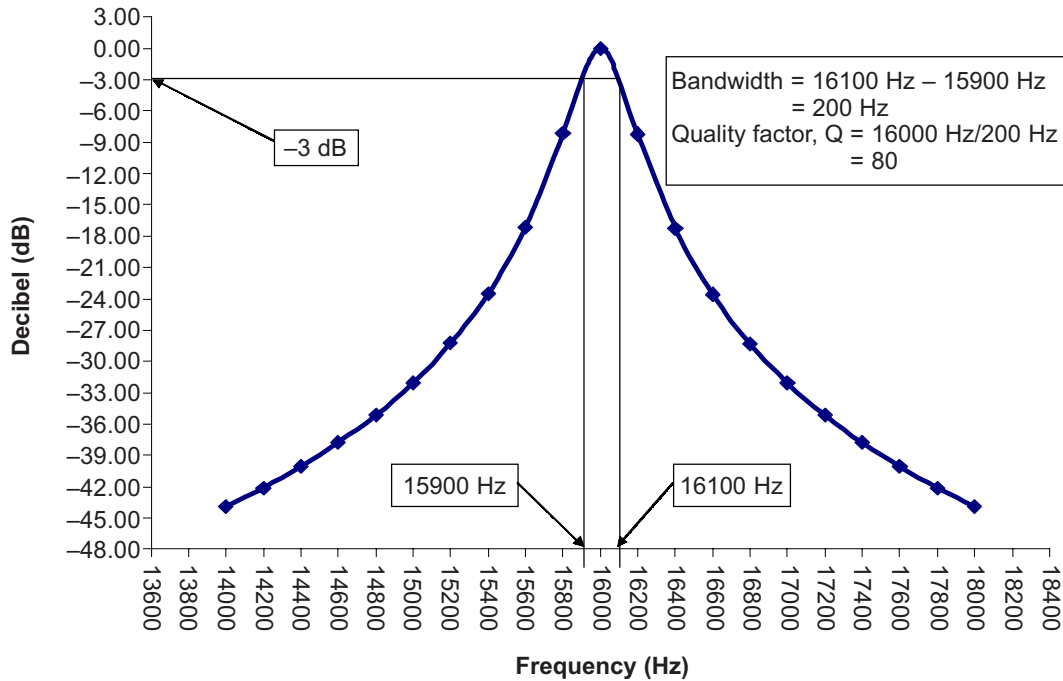
Figure 7   Sound power level for Beam 10 at the range of its applied frequencies

found in Figure 7. Table 3 shows the half power bandwidth and quality factor for different beams.

The half power bandwidth refers to the beam's useful range of operating frequencies. For example from Table 3, the half power bandwidth for Beam 10 was 200 Hz. This means that the useful operating frequencies for Beam 10 were ranged from 15 900 to 16 100 Hz. The band pass filter was used to filter the unwanted frequencies in the simulation. The quality factors for the beams (PZT 5A) were around the value of 80.

4.3   Simulation with SIMULINK®

Simulation using SIMULINK® software was undertaken to obtain sound power level of the beams (Figure 8). The sound frequencies were inserted as input frequency. The beams could detect the input frequencies that were the same with the resonant frequency of the beams or located in the half power bandwidth of the beams. The electric potential produced by the beam was converted to sound power level as output. Table 4 shows the output result for five input frequencies from simulation using SIMULINK®.

Table 4   Output result for five input frequencies in the simulation using SIMULINK®

Input frequency (Hz)	Detected beam	Sound power level (dB)
126	Beam 3	–4.40
505	Beam 5	–6.10
990	Beam 6	–6.03
8050	Beam 9	–4.13
15950	Beam 10	–2.04

5.0   CONCLUSION

Piezoelectric acoustic microsensor could be used to detect sound signals at the octave band frequency ranging from 31.5 Hz to 16 kHz. The decreasing of the beam's length caused the resonant frequency for the beam to increase and this is similar to the performance of the outer hair cells (OHCs) inside human ears. The maximum electric potential produced by long beam at its resonant frequency is higher than the short beam under similar condition.

Piezoelectric acoustic microsensor produced by PZT 5A has micrometer sized, high sensitivity, high permittivity, high frequency responses, high time stability and can be used as sound detector in various applications such as microphone or sound recognition system. The piezoelectric acoustic microsensor can indicate the sound signals at the octave frequencies directly without Fast Fourier Transform (FFT).

ACKNOWLEDGEMENTS

REFERENCES

[1]   Aldraihem, O. J., and A. A. Khdeir. 2002. Exact Deflection Solutions of Beams with Shear Piezoelectric Actuators. *J. Solids and Structures*. 40: 1-12.

[2]   Rajapakse, R. K. N. D. 1997. Plane Stain/Stress Solutions for Piezoelectric Solids. *J. Composites Part B*. 2B: 385-396.

[3]   Wan, J. G., and B. Q. Tao. 2000. Design and Study on a 1-3 Anisotropy Piezocomposite Sensor. *J. Materials and Design*. 21: 533-536.

[4]   Fung, R. F., S. C. Chao, and Y. S. Kung. 2001. Piezothermoelastic Analysis of an Optical Beam Defector. *J. Sensors and Actuators A*. 87: 179-187.

[5]   Gaudenzi, P., R. Carbonaro, and R. Barboni. 1997. Vibration Control of an Active Laminated Beam. *J. Composite Structures*. 38(1-4): 413-420.

[6]   Luo, Q., and L. Tong. 2002. Exact Static Solutions to Piezoelectric Smart Beams Including Peel Stresses I: Theoretical Formulation. *J. Solids and Structures*. 39: 4677-4695.

[7]   Paczelt, I., and P. Z. Kovacs. 2000. Finite Element Investigation of an Adaptive Cantilever Plate. CDROM Proceedings of the 8th International Conference on Numerical Methods in Continuum Mechnics 2000. University of Zilina, Slovak Republic.

[8]   Pietrzakowki, M. 2001. Active Damping of Beams by Piezoelectric System: Effects of Bonding Layer Properties. *J. Solids and Structures*. 38: 7885-7897.

[9]   Waisman, H., and H. Abramovich. 2002. Active Stiffening of Laminated Composite Beams Using Piezoelectric Actuators. *J. Composite Structures*. 58: 109-120.

[10] Xu, C. H., J. H. Hu, and H. L. W. Chan. 2002. Behavior of a PZT Ring under Non-uniform Mechanical Stress. *J. Ultrasonics*. 39: 735-742.

[11] Xu, X. L., and R. K. N. D. Rajapakse. 1998. Boundary Element Analysis of Piezoelectric Solids with Defects. *J. Composites Part B*. 29B: 655-669.

[12] Yang, R. B., and J. H. Huang. 2002. Fracture Analysis of Piezoelectric Materials with Flat Ellipsoidal Cracks. *J. Materials Letters*. 57: 481-489.

[13] Gruebner, O., M. Kamlah, and D. Munz. 2002. Finite Element Analysis of Cracks in Piezoelectric Materials Taking into Account the Permittivity of the Crack Medium. *J. Engineering Fracture Mechanics*. 70: 1399-1413.

[14] Dufaud, O., P. Marchal, and S. Corbel. 2002. Rheological Properties of PZT Suspensions for Stereolithography. *J. European Ceramic Society*. 22: 2081-2092.

[15] Huang, H. M., H. J. Shi, and Y. J. Yin. 2002. Multi-cracks Problem for Piezoelectric Materials Strip Subjected to Dynamic Loading. *J. Mechanics Research Communications*. 29: 413-424.

[16] Benjeddou, A. 2000. Advances in Piezoelectric Finite Element Modeling of Adaptive Structural Elements: A Survey. *J. Computers and Structures*. 76: 347-363.

[17] Chen, L. W., C. Y. Lin, and C. C. Wang. 2002. Dynamics Stability Analysis and Control of a Composite Beam with Piezoelectric Layers. *J. Composite Structures*. 56: 97-109.

[18] Huang, D., and B. H. Sun. 2001. Approximate Solution on Smart Composite Beams by Using MATLAB. *J. Composite Structures*. 54: 197-205.

[19] Liu, Y., and H. Fan. 2002. Analysis of Thin Piezoelectric Solids by the Boundary Element Method. *J. Comput. Methods Appl. Mech. Engrg*. 191: 2297-2315.

[20] Mukherjee, A., and A. S. Chaudhuri. 2002. Piezolaminated Beams with Large Deformations. *J. Solids and Structures*. 39: 4567-4582.

[21] Shang, F., M. Kuna, and M. Abendroth. 2003. Finite Element Analyses of Three-dimensional Crack Problems in Piezoelectric Structures. *J. Engineering Fracture Mechanics*. 70: 143-160.

[22] Sun, B., and D. Huang. 2001. Vibration Suppression of Laminated Composite Beams with a Piezoelectric Damping Layer. *J. Composite Structures*. 53: 437-447.

[23] Sunar, M., S. J. Hyder, and B. S. Yilbas. 2001. Robust Design of Piezoelectric Actuators for Structural Control. *J. Comput. Methods Appl. Mech. Engrg*. 190: 6257-6270.

[24] Sze, K. Y., H. T. Wang, and H. Fan. 2001. A Finite Element Approach for Computing Edge Singularities in Piezoelectric Materials. *J. Solids and Structures*. 38: 9233-9252.

[25] Wu, X. H., C. Chen, Y. P. Shen, and X. G. Tian. 2002. A High Order Theory for Functionally Graded Piezoelectric Shells. *J. Solids and Structures*. 39: 5325-5344.

[26] Xiao, Z. M., and J. Bai. 2002. Numerical Simulation on a Coated Piezoelectric Sensor Interacting with a Crack. *J. Finite Elements in Analysis and Design*. 38: 691-706.

[27] Xu, X. L., and R. K. N. D. Rajapakse. 2001. On a Plane Crack in Piezoelectric Solids. *J. Solids and Structures*. 38: 7643-7658.

[28] Abramovich, H., and H. R. Meyer-piening. 1998. Induced Vibrations of Piezolaminated Elastic Beams. *J. Composite Structures*. 43: 47-55.

[29] Melnik, R. V. N. 2000. Generalised Solutions, Discrete Models and Energy Estimates for a 2D Problem of Coupled Field Theory. *J. Applied Mathematics and Computation*. 107: 27-55.

[30] Melnik, R. V. N. 2002. Numerical Analysis of Dynamic Characteristics of Coupled Piezoelectric Systems in Acoustic Media. *J. Mathematics and Computers in Simulation*. 2129: 1-11.

[31] Langemry, L. 2002. *FEMLAB Structural Mechanics Module*. Version 2.3. Sweden: COMSOLAB.

[32] Beckwith, T. G., R. D. Marangoni, and J. H. Lienhard. 1993. *Mechanical Measurements*. 5th ed. Reading, Massachusetts: Addison-Wesley Publishing Company.

[33] Johnson, K. 1997. *Acoustic & Auditory Phonetics*. Cambridge, Massachusetts: Blackwell Publishers Inc.

[34] French, A. P. 1995. *Vibrations and Waves*. London: Chapmen & Hall.

[35]   Brownell, W. E., A. A. Spector, R. M. Raphael, and A. S. Popel. 2001. Micro and Nanomechanics of the
        Cochlear Outer Hair Cell. *J. Biomed. Eng.* 3: 169-194.

[36]   Brownell, W. E. 2001. On the Origins of Outer Hair Cell Electromotility. In *Hair Cell Micromechanics and
        Otoacoustic Emissions*. Edited by Berlin *et al*. Albany, NY: Delmar-Thomson Learning.

[37]   Halter, J. A., R. P. Kruger, M. J. Yium, and W. E. Brownell. 1997. The Influence of the Subsurface
        Cisterna on the Electrical Properties of the Outer Hair Cell. *Rapid Science Publishers, NeuroReport*.
        8: 2517-2521.

[38]   Li, Z. W., B. Anvari, M. Takashima, P. Brecht, J. H. Torres, and W. E. Brownell. 2002. Membrane Tether
        Formation from Outer Hair Cells with Optical Tweezers. *Biophysical J.* 82: 1386-1395.

[39]   Lue, J. C., H. B. Zhao, and W. E. Brownell. 2001. Chlorpromazine Alters Outer Hair Cell Electromotility.
        American Academy of Otolaryngology-Head and Neck Surgery Foundation Inc. Otolaryngol Head Neck Surg.
        125: 71-76.

[40]   Raphael, R. M., A. S. Popel, and W. E. Brownell. 2000. A Membrane Bending Model of Outer Hair Cell
        Electromotility. *Biophysical J.* 78: 2844-2862.

[41]   Conrad, J., and Jr. Hemond. 1983. *Engineering Acoustics & Noise Control*. NJ: Prentice- Hall Inc.

[42]   Arafa, M., and A. Baz. 2000. Dynamics of Active Piezoelectric Damping Composites. *J. Composites*,
        Part B. 31: 255-264.

[43]   CTS$_\circledR$ Wireless Components Report. 2000. PZT Piezoelectric Materials: Technical Data (Typical Values).
        CTS$_\circledR$.

[44]   Giannakopoulos, A. E., and S. Suresh. 1999. Theory of Indentation of Piezoelectric Materials.
        Acta Metallurgica Inc. Acta Mater. 47: 2153-2164.

[45]   Morris, C. J., and F. K. Forster. 2000. Optimization of a Circular Piezoelectric Bimorph for a Micropump
        Driver. *J. Micromech. Microeng*. 10: 459-465.